8-1-2019

The Distal Cytoplasmic Tail Of The Influenza A M2 Protein Dynamically Extends From The Membrane

Grace Kim , '17

Hayley E. Raymond , '18

Alice L. Herneisen , '17

See next page for additional authors

Recommended Citation

Grace Kim , '17; Hayley E. Raymond , '18; Alice L. Herneisen , '17; Abigail Wong-Rolle , '19; and Kathleen P. Howard. (2019). "The Distal Cytoplasmic Tail Of The Influenza A M2 Protein Dynamically Extends From The Membrane". *Biochimica Et Biophysica Acta: Biomembranes.* Volume 1861, Issue 8. 1421-1427. DOI: 10.1016/j.bbamem.2019.05.021
https://works.swarthmore.edu/fac-chemistry/240

Published in final edited form as:

Biochim Biophys Acta Biomembr. 2019 August 01; 1861(8): 1421–1427. doi:10.1016/j.bbamem.2019.05.021.

The distal cytoplasmic tail of the Influenza A M2 protein dynamically extends from the membrane

Grace Kim[†,1], **Hayley E. Raymond**[†,1], **Alice L. Herneisen**[†,2], **Abigail Wong-Rolle**[†], and **Kathleen P. Howard**[†,*]

[†]Department of Chemistry and Biochemistry, Swarthmore College, Swarthmore, PA 19081

Abstract

The influenza A M2 protein is a multifunctional membrane-associated homotetramer that orchestrates several essential events in the viral infection cycle. The monomeric subunits of the M2 homotetramer consist of an N-terminal ectodomain, a transmembrane domain, and a C-terminal cytoplasmic domain. The transmembrane domain forms a four-helix proton channel that promotes uncoating of virions upon host cell entry. The membrane-proximal region of the C-terminal domain forms a surfaceassociated amphipathic helix necessary for viral budding. The structure of the remaining ~34 residues of the distal cytoplasmic tail has yet to be fully characterized despite the functional significance of this region for influenza infectivity. Here, we extend structural and dynamic studies of the poorly characterized M2 cytoplasmic tail. We used SDSL-EPR to collect site-specific information on the mobility, solvent accessibility, and conformational properties of residues 61–70 of the full-length, cell-expressed M2 protein reconstituted into liposomes. Our analysis is consistent with the predominant population of the C-terminal tail dynamically extending away from the membranes surface into the aqueous medium. These findings provide insight in hypotheses than the C-terminal domain serves as a sensor of changes in both membrane composition and binding of other viral proteins that helps regulate how the multifunctional M2 protein participates in critical events in the viral infection cycle.

Graphical Abstract

[*]Corresponding Author: khoward1@swarthmore.edu.
[1]Contributed equally to this work.
[2]Current Address: Biology Department, MIT

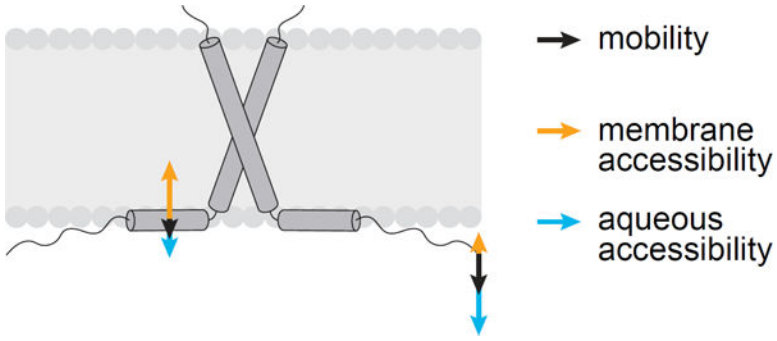

Keywords

full-length Influenza A M2 protein; cytoplasmic tail; site-directed spin labeling; electron paramagnetic resonance

1. Introduction

The influenza A virus causes seasonal epidemics and global pandemics, thereby posing a critical public health risk [1]. An atomic-level understanding of each step of the viral life cycle could inform new antiviral strategies. The influenza A M2 protein is a multifunctional membrane-associated homotetramer that orchestrates several essential events in the viral infection cycle, such as viral assembly and budding [2,3]. Here, we extend structural and dynamic studies of the poorly characterized M2 cytoplasmic tail.

The monomeric subunits of the M2 homotetramer consist of an N-terminal ectodomain, a transmembrane domain, and a C-terminal cytoplasmic domain (Figure 2A). The transmembrane domain forms a four-helix proton channel that promotes uncoating of virions upon host cell entry [2]. The C-terminal domain regulates viral budding and morphology [3], proton-channel activity [4], and viral assembly through interactions with other influenza virus proteins including the matrix protein M1 [5]. The membrane-proximal region of the C-terminal domain forms a surface-associated amphipathic helix. The structure of the remaining ~34 residues of the distal cytoplasmic tail has yet to be fully characterized despite the functional significance of this region for influenza infectivity.

The functional significance of the distal cytoplasmic tail of M2 protein has been elucidated by several lines of inquiry. A series of deletion mutants of the M2 cytoplasmic tail demonstrated the region had a large impact the assembly of progeny virions [6]. C-terminal truncations led to reduced nucleoprotein incorporation into virions and altered filament formation on virus-infected cells. The interaction of M2 with matrix protein 1 (M1) has been shown to be critical to the viral replication cycle with the putative binding site near residues 71–76 within the M2 cytoplasmic tail [6–10]. Evidence for the complementary roles of the M1 and M2 proteins in virus assembly has been provided by identification of M1 suppressor mutations that complement a lethal tyrosine-to-alanine M2 mutation at amino acid 76 [7]. Detailed biophysical work has focused on the ability of the C-terminal amphipathic helix of M2 to induce curvature necessary for the viral budding and scission [11–13]. However, it is

has also been shown that while the amphipathic helix can generate curvature on its own, the full-length M2 protein is more efficient at generating curvature suggesting the C-terminal tail is acting synergistically with the amphipathic helix to induce membrane curvature [12].

The M2 protein has been studied by a range of biophysical techniques, including X-ray crystallography [14], solution NMR [15], solid-state NMR (ssNMR) [16–18] and site-directed spin label electron paramagnetic resonance (SDSL-EPR) spectroscopy [19–25]. Until recently, the majority of M2 biophysical studies utilized chemically synthesized, truncated constructs that omit the functionally significant cytoplasmic tail domain. The most frequently studied constructs include the transmembrane domain peptide (M2TM, residues ~22–46) or the transmembrane domain with the Cterminal amphipathic helix extension (M2TMC, residues ~22–62).

Here, we use SDSL-EPR, a technique exquisitely suited for detecting the mobility and membrane topology of membrane proteins reconstituted into liposomes [26], to collect site-specific information on the mobility, solvent accessibility, and conformational properties of residues 61–70 of the full-length, cell-expressed M2 protein. In previous studies of full length M2, we characterized the multicomponent nature of M2-WT CW line shapes for sites 50–60 in the C-terminal amphipathic helix and established that they arose from an equilibrium involving two different conformational substates of the protein. Line shapes for sites 62–70 also show evidence of a superposition of two states, although the component arising from the highly mobile population dominates the spectra. Compared to the amphipathic helix proximal to the transmembrane domain, the dominant population of the C-terminal tail is more dynamic and has moved away from the membrane surface into the aqueous phase. The ability to measure both mobility and membrane accessibility parameters of specific sites provides insight into where the membrane-associated amphipathic helix ends. The conformational and dynamic properties of the C-terminal tail beyond the amphipathic helix reported here provide valuable conformational insight into a region of M2 protein known to have a critical role in the regulation of viral assembly and budding.

2. Materials and Methods

2.1 Sample preparation

Single cysteine substitutions were introduced into a cysteineless background plasmid based on the A/Udorn/72 M2 sequence [27] using site-directed mutagenesis. Expression, purification, and spin labelling were performed according to previously published protocols [22,25].

Protein was reconstituted into 4:1 1-palmitoyl-2-oleoyl-snglycero- 3-phosphocholine/ palmitoyl-2-oleoyl-sn-glycero-3-phospho-1-rac-glycerol lipid bilayers as previously described [28]. This membrane system was chosen for its use in in vitro budding assays [29] and previous SDSL-EPR studies of the M2 protein [20–25]. The buffer used for collection of mobility data and oxygen accessibility measurements was 50 mM Tris pH 7.8, 100 mM KCl, and 1 mM EDTA. The buffer for nickel (II) ethylenediaminediacetate (NiEDDA) accessibility studies was 50 mM NiEDDA, 50 mM Tris pH 7.8, and 100 mM KCl buffer. At pH 7.8 the M2 proton channel does not conduct protons and is in the closed state [2].

2.2 EPR Spectroscopy and Data Analysis.

Continuous wavelength (CW) EPR spectra were recorded on an X-band Bruker EMX spectrometer equipped with an ER4123S resonator at room temperature. Samples were placed in 0.6 mm internal diameter, 0.9 mm length gas permeable capillary tubes (L&M EPR Supplies, Milwaukee, WI). CW EPR spectra were acquired using 2 mW incident microwave power, 1 G field modulation amplitude at 100 kHz, and 150 G sweep width.

Power saturation experiments were used to probe the membrane depth of residues. Experiments were collected in the presence of two different paramagnetic relaxation agents, O_2 and NiEDDA. Oxygen is a lipophilic species that partitions in a gradient across the membrane, with the highest O_2 concentration at the center of the bilayer. NiEDDA is water-soluble paramagnetic relaxation agent which is used to measure the accessibility of spin-labeled sites to the aqueous phase. Accessibility experiments were collected under three conditions: equilibrated with ambient air, equilibrated with nitrogen gas, and equilibrated with nitrogen in the presence of NiEDDA. Nitrogen power saturation experiments were collected over 8 power levels. All other power saturation experiments were measured over at least 16 power levels. Data were fit to obtain $\Delta P_{1/2}$ parameters as described previously [20]. Sites with very high accessibility to NiEDDA were not saturated at the powers obtainable. Thus, $\Delta P_{1/2}$(NiEDDA) values greater than 200 should be considered estimates. The contrast parameter, ϕ, was calculated according to the following equation[30]:

$$\phi = ln\left(\frac{\Delta P_{\frac{1}{2}}(O_2)}{\Delta P_{\frac{1}{2}}(\mathrm{NiEDDA})}\right)$$

3. Results

3.1 Dominant population of the C-terminal tail is highly dynamic beyond the amphipathic helix

The EPR spectral line shapes of spin-labeled residues provide insight into conformational dynamics that reflect both backbone motion as well as secondary and tertiary contacts [26]. EPR line shapes for residues 61–70 are shown in Figure 1. For comparison, previously reported CW line shapes for sites 50–60 [22] are shown to highlight the marked change in line shapes past the residues closest to the end of the transmembrane domain.

The line shapes for amphipathic helix residues 50–61 are distinctly broader than 62–70. The 50–61 spectra are a superposition of a broad, immobilized component (i), and a sharper, mobile component (m). In previous studies of M2, we characterized the multicomponent nature of the C-terminal amphipathic helix using both line shape analysis and saturation recovery methods to establish the presence of an equilibrium involving two different conformational substates of the protein. We hypothesized that this conformational exchange is relevant for M2 scission function at the edge of the viral budozone[24,25].

Similar to sites 50–60, line shapes for sites 62–70 show evidence of a superposition of two states, although the component arising from a mobile population dominates the spectra. The

dynamics of a spin-labeled site can be qualitatively assessed using a semi-empirical mobility factor calculated from the inverse peak-to-peak width of the central line (ΔH_0^{-1}) of the EPR line shapes [26]. Mobility factors were calculated from the CW-EPR spectra of each site. In the case of multicomponent spectra, the mobility factors reflect the properties of the overlapping components and provide only a qualitative measure of average dynamics at the site. Nonetheless, mobility factors along a stretch of neighboring residues can provide useful insight into changes in dynamic properties in a specific region of the protein. Mobility as a function of M2 sequence position is shown in Figure 2B with previously reported data for sites 50–60 within the amphipathic helix for comparison [22]. The mobility of sites 50–60 is low, consistent with restrictions in motion arising from a membrane surface-associated secondary structural element. Mobility factors in the range of 0.2–0.4 have been reported for spin labeled sites within α-helical secondary structure elements within membrane associated proteins[31,32]. In marked contrast to 50–60, spin labels at positions 61–70 exhibit a gradient of increasing mobility.

3.2 The dominant population of the C-terminal tail extends away from the membrane surface

Spin label motional restriction can arise from secondary and tertiary contacts or association with the membrane [26]. Previously, we established that residues 50–60 of the full-length M2 protein form an amphipathic helix associated with the membrane surface. Here, we tested the hypothesis that the observed increase in mobility for sites 61–70 could be attributed to a loss of association with the membrane surface.

We conducted power saturation experiments to measure accessibility to the paramagnetic relaxation agent O_2 which reports on structural topology with respect to the membrane. Oxygen is a lipophilic species that partitions in a gradient across the membrane, with the highest O_2 concentration at the center of the bilayer. The collision rate of the spin label with O_2, quantified by $\Delta P_{1/2}$ (O_2), serves as a relative measurement of membrane accessibility [26].

Oxygen accessibility as a function of spin-label position for sites 61–70 is presented in Figure 2C along with previously published data for 50–60 for comparison [22]. The overall trend is one of decreasing oxygen accessibility towards the distal cytoplasmic tail, a hallmark of increasing distance from the membrane.

3.3 Conformational properties of the C-terminal tail beyond the amphipathic helix

While O_2 accessibility provides information about the depth of a particular site in the membrane environment, $\Delta P_{1/2}(O_2)$ data can be difficult to interpret for residues positioned near the lipid head groups or in the aqueous environment. To better characterize sites along the membraneaqueous interface, we employed a water-soluble paramagnetic relaxation agent, NiEDDA, which is used to measure the accessibility of spin-labeled sites to the aqueous phase [26]. Hydrophobic O_2 and hydrophilic NiEDDA have opposite membrane partitioning tendencies. Consistent with these partitioning tendencies, there is a general trend of increasing NiEDDA accessibility between sites 60 and 70 (Figure 3A), while the trend is one of decreasing oxygen accessibility (Figure 3B).

Oscillations in O_2 and NiEDDA accessibilities have been shown to be indicators of secondary structural elements [26]. Residue-by-residue patterns in accessibility to O_2 and NiEDDA can provide a topological map of secondary structure with respect to the membrane [26]. Previous analysis of positions 50–60 in full-length M2 identified a sinusoidal variation in oxygen accessibility with a periodicity of 3.6, characteristic of a surface-associated α-helix [22]. As a general trend, we observed that the NiEDDA and O_2 accessibilities of sites 60–63 oscillate 180 out of phase (Figure 3A and 3B). Previous work has demonstrated that presence of secondary structure can be usefully predicted by the calculation of a contrast parameter, Φ, that combines accessibilities of O_2 and NiEDDA for a given site [30]. Membrane-buried sites display spikes in Φ values whereas regions that are homogenously solvated in the aqueous phase exhibit relatively constant Φ values [30]. As shown in Figure 3C, the contrast parameters for sites 60–64 oscillate as expected for being part of an amphipathic helix and have magnitudes comparable to those reported for other membrane associated proteins [33,34]. The contrast parameters for sites 65–70 exhibit little variation. Together with the mobility parameters of these residues (Figure 2B), the EPR data suggest that sites 65–70 form a dynamic and predominantly disordered region that extends away from the membrane into the aqueous medium. Due to the existence of two components in the line shapes shown in Figure 1 we are unable to discount the existence of a minor population of ordered secondary structure that is not apparent in the contrast parameters.

4. Discussion

Until recently, the majority of biophysical studies on the M2 protein from influenza A largely focused on the transmembrane domain and the C-terminal amphipathic helix extension using chemical synthesize truncated constructs. The contribution of this paper is to provide information on the distal cytoplasmic tail in full-length M2 protein reconstituted in liposomes.

SDSL-EPR line shapes shows that the C-terminal domain region past the amphipathic helix has evidence for two components, with the predominate population being highly dynamic and extending away from the membrane surface. The site-specific resolution of EPR mobility membrane accessibility data provides valuable insight into where the amphipathic helix ends. The oscillatory pattern in accessibility data suggests the amphipathic helix extends out to residue 64. The EPR data agree with the literature on amino acid sequences typically found at the end of helical regions. The pattern of a glycine followed by a proline (found in 63–64 in the M2 sequence studied here) is a common component of capping motifs prevalent in the C-termini of alpha helices [35].

Our finding that the region beyond the amphipathic region is highly mobile is consistent with earlier ssNMR work [36,37]. An study using chemical shift simulation proposed that unassigned ssNMR peaks from full-length M2 protein arose from an unstructured cytoplasmic tail [36]. A follow-up study on a chemically synthesized truncation that included ~10 residues beyond to the amphipathic helix, M2(22–71), concluded that the post-amphipathic helix cytoplasmic tail up to residue 71 was disordered and highly dynamic [37]. Our SDSL-EPR approach offers advantages over the previously published work on the C-terminal tail of M2. We use full-length M2 protein that includes the entire cytoplasmic tail,

whereas the other study that offers site-specific data [20] utilized a truncated construct, M2 (22–71). Furthermore, we collected data at a 1:500 peptide:lipid ratio, in contrast to the high peptide:lipid ratios (~1:20) required for ssNMR studies, which can complicate the interpretation of data due to potential intermolecular interactions.

It has been hypothesized that the C-terminal tail of M2 helps regulate the multiple roles M2 plays in the influenza viral life cycle [12,38]. The M2 protein is embedded in membrane environments that differ in content depending on the stage of the infection cycle. For example, the influenza virus envelope is enriched in cholesterol compared to the host-cell membrane where M2 facilitates viral budding [3]. Biophysical studies have shown that the conformation and dynamics of the C-terminal domain of M2 differ depending on the membrane context [25,36]. A dynamic cytoplasmic tail may serve as a sensor of changes in membrane composition, as well as the presence of other viral proteins, [36].

Matrix protein 1 (M1) has been proposed to be interact with the C-terminal tail of M2 as part of nucleoprotein incorporation into virions and formation of virions on virus-infected cells. It has been hypothesized that a coli-to-helix conformational change in the C-terminal tail of M2 in the presence of M1 protein might facilitate the M1-M2 interaction [37]. The two populations of EPR line shapes we see in the EPR line shapes for sites 61–70 reported here support the hypothesis that M2 populates different conformational states, where the predominant population of the C-terminal tail under the sample conditions used here dynamically extends away from the membrane surface into the aqueous medium. The minor population we see here could be the one primarily populated in the presence of M1 protein. The hypothesis that the M2 protein has multiple low-energy conformational states is not new [24,39,40]. It has been suggested that the various structural models proposed to date provide snapshots of distinct conformational states sampled by the protein during the viral life cycle [19,23]. The M2 protein has at least two functions, the proton channel activity crucial for uncoating of virions [2] and the formation of virions on virus-infected cells [3]. The different functions of M2 could conceivably require different conformations. Ongoing conformational studies under conditions relevant to viral budding and in the presence of M1 protein will further inform how the C-terminal tail of the M2 protein participates in the viral lifecycle.

5. Conclusions

Until recently, the majority of M2 biophysical studies utilized chemically synthesized, truncated constructs that omit the functionally significant cytoplasmic tail domain. The contribution of this paper is to provide information on the cytoplasmic tail in full-length M2 protein. We used SDSL-EPR to collect site-specific information on the mobility, solvent accessibility, and conformational properties of residues 61–70 of the full-length, cell-expressed M2 protein reconstituted into liposomes. Compared to the C-terminal domain amphipathic helix proximal to the transmembrane domain, the dominant population of the distal cytoplasmic tail is more dynamic and has moved away from the membrane surface into the aqueous phase. Evidence for two conformations of the C-terminal tail is consistent with previous studies that demonstrates that under different sample conditions, M2 populates different states linked to different roles M2 plays in the viral lifecycle [24,39,40]. The C-

terminal cytoplasmic tail could be a sensor of changes in both membrane composition and binding of other viral proteins, thus regulating the multiple essential roles of M2 in the influenza infection cycle.

Supplementary Material

Refer to Web version on PubMed Central for supplementary material.

Acknowledgments

Funding. This work was generously supported by NIH grant AI117657–01 to KPH.

Abbreviations.

SDSL-EPR	site-directed spin labeling electron paramagnetic resonance spectroscopy
ssNMR	solid-state NMR
TM	transmembrane
AH	amphipathic helix
POPC	1-palmitoyl-2-oleoyl-snglycero-3-phosphocholine
POPG	1-palmitoyl-2-oleoyl-sn-glycero-3-phospho-1-rac-glycerol
CW EPR	continuous-wave electron paramagnetic resonance
NiEDDA	nickel (II) ethylenediaminediacetate

References

[1]. Petrova VN, Russell CA, The evolution of seasonal influenza viruses, Nature Reviews Microbiology, (2018) 47–60. [PubMed: 29081496]

[2]. Pinto LH, Lamb RA, The M2 proton channels of influenza A and B viruses, Journal of Biological Chemistry, 281 (2006) 8997–9000. [PubMed: 16407184]

[3]. Rossman JS, Lamb RA, Influenza virus assembly and budding, Virology, 411 (2011) 229–236. [PubMed: 21237476]

[4]. Liao SY, Yang Y, Tietze D, Hong M, The Influenza M2 Cytoplasmic Tail Changes the Proton-Exchange Equilibria and the Backbone Conformation of the Transmembrane Histidine Residue to Facilitate Proton Conduction, Journal of the American Chemical Society, 137 (2015) 6067–6077. [PubMed: 25892574]

[5]. McCown MF, Pekosz A, Distinct domains of the influenza A virus M2 protein cytoplasmic tail mediate binding to the M1 protein and facilitate infectious virus production, Journal of Virology, 80 (2006) 8178–8189. [PubMed: 16873274]

[6]. Iwatsuki-Horimoto K, Horimoto T, Noda T, Kiso M, Maeda J, Watanabe S, Muramoto Y, Fujii K, Kawaoka Y, The cytoplasmic tail of the influenza A virus M2 protein plays a role in viral assembly, Journal of Virology, 80 (2006) 5233–5240. [PubMed: 16699003]

[7]. Liu H, Grantham ML, Pekosz A, Mutations in the Influenza A virus M1 protein enhance virus budding to complement lethal mutations in the M2 cytoplasmic tail, Journal of Virology, 92 (2018) 1–14.

[8]. Chen BJ, Leser GP, Jackson D, Lamb RA, The influenza virus M2 protein cytoplasmic tail interacts with the M1 protein and influences virus assembly at the site of virus budding, Journal of Virology, 82 (2008) 10059–10070. [PubMed: 18701586]

[9]. Zebedee SL, Lamb R. a, Growth restriction of influenza A virus by M2 protein antibody is genetically linked to the M1 protein, Proceedings of the National Academy of Sciences, 86 (1989) 1061–1065.

[10]. McCown MF, Pekosz A, The Influenza A Virus M 2 Cytoplasmic Tail Is Required for Infectious Virus Production and Efficient Genome Packaging, J. Virol, 79 (2005) 3595–3605. [PubMed: 15731254]

[11]. Roberts KL, Leser GP, Ma CL, Lamb RA, The amphipathic helix of influenza A virus M2 protein is required for filamentous bud formation and scission of filamentous and spherical particles, Journal of Virology, 87 (2013) 9973–9982. [PubMed: 23843641]

[12]. Schmidt NW, Mishra A, Wang J, Degrado WF, Wong GCL, Influenza Virus A M2 Protein Generates Negative Gaussian Membrane Curvature Necessary for Budding and Scission, Journal of the American Chemical Society, 135 (2013) 13710–13719. [PubMed: 23962302]

[13]. Martyna A, Bahsoun B, Badham MD, Srinivasan S, Howard MJ, Rossman JS, Membrane remodeling by the M2 amphipathic helix drives influenza virus membrane scission, Scientific Reports, 7 (2017) 44695. [PubMed: 28317901]

[14]. Thomaston JL, Alfonso-Prieto M, Woldeyes RA, Fraser JS, Klein ML, Fiorin G, DeGrado WF, High-resolution structures of the M2 channel from influenza A virus reveal dynamic pathways for proton stabilization and transduction, Proceedings of the National Academy of Sciences, 112 (2015) 14260–14265.

[15]. Claridge JK, Aittoniemi J, Cooper DM, Schnell JR, Isotropic bicelles stabilize the juxtamembrane region of the influenza M2 protein for solution NMR studies, Biochemistry, 52 (2013) 8420–8429. [PubMed: 24168642]

[16]. Sharma M, Yi M, Dong H, Qin H, Peterson E, Busath DD, Zhou H-X, Cross TA, Insight into the Mechanism of the Influenza A Proton Channel from a Structure in a Lipid Bilayer, Science, 330 (2010) 509–512. [PubMed: 20966252]

[17]. Cady SD, Wang J, Wu Y, DeGrado WF, Hong M, Specific binding of adamantane drugs and direction of their polar amines in the pore of the influenza M2 transmembrane domain in lipid bilayers and dodecylphosphocholine micelles determined by NMR spectroscopy, J Am Chem Soc, 133 (2011) 4274–4284. [PubMed: 21381693]

[18]. Andreas LB, Eddy MT, Pielak RM, Chou J, Griffin RG, Magic Angle Spinning NMR Investigation of Influenza A M2 $_{18–60}$: Support for an Allosteric Mechanism of Inhibition, Journal of the American Chemical Society, 132 (2010) 10958–10960. [PubMed: 20698642]

[19]. Duong-Ly KC, Nanda V, Degrado WF, Howard KP, Degrad WF, Howard KP, Degrado WF, Howard KP, The conformation of the pore region of the M2 proton channel depends on lipid bilayer environment, Protein Science, 14 (2005) 856–861. [PubMed: 15741338]

[20]. Nguyen PA, Soto CS, Polishchuk A, Caputo GA, Tatko CD, Ma CL, Ohigashi Y, Pinto LH, DeGrado WF, Howard KP, pH-induced conformational change of the influenza M2 protein C-terminal domain, Biochemistry, 47 (2008) 9934–9936. [PubMed: 18754675]

[21]. Thomaston JL, Nguyen PA, Brown EC, Upshur MA, Wang J, DeGrado WF, Howard KP, Detection of drug-induced conformational change of a transmembrane protein in lipid bilayers using site-directed spin labeling, Protein Science, 22 (2013) 65–73. [PubMed: 23139077]

[22]. Huang S, Green B, Thompson M, Chen R, Thomaston J, DeGrado WF, Howard KP, C-terminal juxtamembrane region of full-length M2 protein forms a membrane surface associated amphipathic helix, Protein Science: A Publication of the Protein Society, 24 (2015) 426–429. [PubMed: 25545360]

[23]. Saotome K, Duong-Ly KC, Howard KP, Influenza A M2 protein conformation depends on choice of model membrane, Peptide Science, 104 (2015) 405–411. [PubMed: 25652904]

[24]. Kim SS, Upshur MA, Saotome K, Sahu ID, McCarrick RM, Feix JB, Lorigan GA, Howard KP, Cholesterol-Dependent Conformational Exchange of the C-Terminal Domain of the Influenza A M2 Protein, Biochemistry, 54 (2015) 7157–7167. [PubMed: 26569023]

[25]. Herneisen AL, Sahu ID, McCarrick RM, Feix JB, Lorigan GA, Howard KP, A Budding-Defective M2 Mutant Exhibits Reduced Membrane Interaction, Insensitivity to Cholesterol, and Perturbed Interdomain Coupling, Biochemistry, 56 (2017) 5955–5963. [PubMed: 29034683]

[26]. Klug CS, Feix JB, Methods and Applications of Site-Directed Spin Labeling EPR Spectroscopy, Methods in Cell Biology, 84 (2008) 617–658. [PubMed: 17964945]

[27]. Leiding T, Wang J, Martinsson J, DeGrado WF, Arskold SP, Proton and cation transport activity of the M2 proton channel from influenza A virus, Proceedings of the National Academy of Sciences of the United States of America, 107 (2010) 15409–15414. [PubMed: 20713739]

[28]. Crouch C, Bost M, Kim T, Green B, Arbuckle D, Grossman C, Howard K, Optimization of Detergent-Mediated Reconstitution of Influenza A M2 Protein into Proteoliposomes, Membranes, 8 (2018) 103 1–12.

[29]. Rossman JS, Jing XH, Leser GP, Lamb RA, Influenza Virus M2 Protein Mediates ESCRT-Independent Membrane Scission, Cell, 142 (2010) 902–913. [PubMed: 20850012]

[30]. Isas JM, Langen R, Haigler HT, Hubbell WL, Structure and dynamics of a helical hairpin and loop region in annexin 12: A site-directed spin labeling study, Biochemistry, (2002).

[31]. Voss J, He MM, Hubbell WL, Kaback HR, Site-Directed Spin Labeling Demonstrates That Transmembrane Domain XII in the Lactose Permease of Escherichia coli Is an R -Helix †, 2960 (1996) 12915–12918.

[32]. Barnakov A, Altenbach C, Barnakova L, Hubbell WL, Hazelbauer GL, Site-directed spin labeling of a bacterial chemoreceptor reveals a dynamic, loosely packed transmembrane domain, (2002) 1472–1481.

[33]. Turner AL, Braide O, Mills FD, Fanucci GE, Long JR, Biochimica et Biophysica Acta Residue speci fi c partitioning of KL 4 into phospholipid bilayers, BBA - Biomembranes, 1838 (2014) 3212–3219. [PubMed: 25251362]

[34]. Altenbach C, Greenhalgh DA, Khorana HG, Hubbell WL, A Collision Gradient-Method to Determine the Immersion Depth of Nitroxides in Lipid Bilayers - Application to Spin-Labeled Mutants of Bacteriorhodopsin, Proceedings of the National Academy of Sciences of the United States of America, 91 (1994) 1667–1671. [PubMed: 8127863]

[35]. Aurora R, Srinivasan R, Rose GD, Rules for α-Helix Termination by Glycine, Science, 264 (1994) 1126–1130. [PubMed: 8178170]

[36]. Liao SY, Fritzsching KJ, Hong M, Conformational analysis of the full-length M2 protein of the influenza A virus using solid-state NMR, Protein Science, 22 (2013) 1623–1638. [PubMed: 24023039]

[37]. Kwon B, Tietze D, White PB, Liao SY, Hong M, Chemical ligation of the influenza M2 protein for solid-state NMR characterization of the cytoplasmic domain, Protein Science, 24 (2015) 1087–1099. [PubMed: 25966817]

[38]. Liao SY, Lee M, Hong M, Interplay between membrane curvature and protein conformational equilibrium investigated by solid-state NMR, Journal of Structural Biology, (2018) 0–1.

[39]. Hu FH, Luo WB, Cady SD, Hong M, Conformational plasticity of the influenza A M2 transmembrane helix in lipid bilayers under varying pH, drug binding, and membrane thickness, Biochimica et Biophysica Acta (BBA) - Biomembranes, 1808 (2011) 415–423. [PubMed: 20883664]

[40]. Yi M, Cross TA, Zhou H-XX, Conformational heterogeneity of the M2 proton channel and a structural model for channel activation, Proceedings of the National Academy of Sciences of the United States of America, 106 (2009) 13311–13316. [PubMed: 19633188]

Highlights

- Dominant population of the C- terminal tail of M2 is highly mobile
- C- terminal tail of M2 extends away from the membrane surface into the aqueous phase
- Mobility and accessibility report on length of membrane- associated amphipathic helix

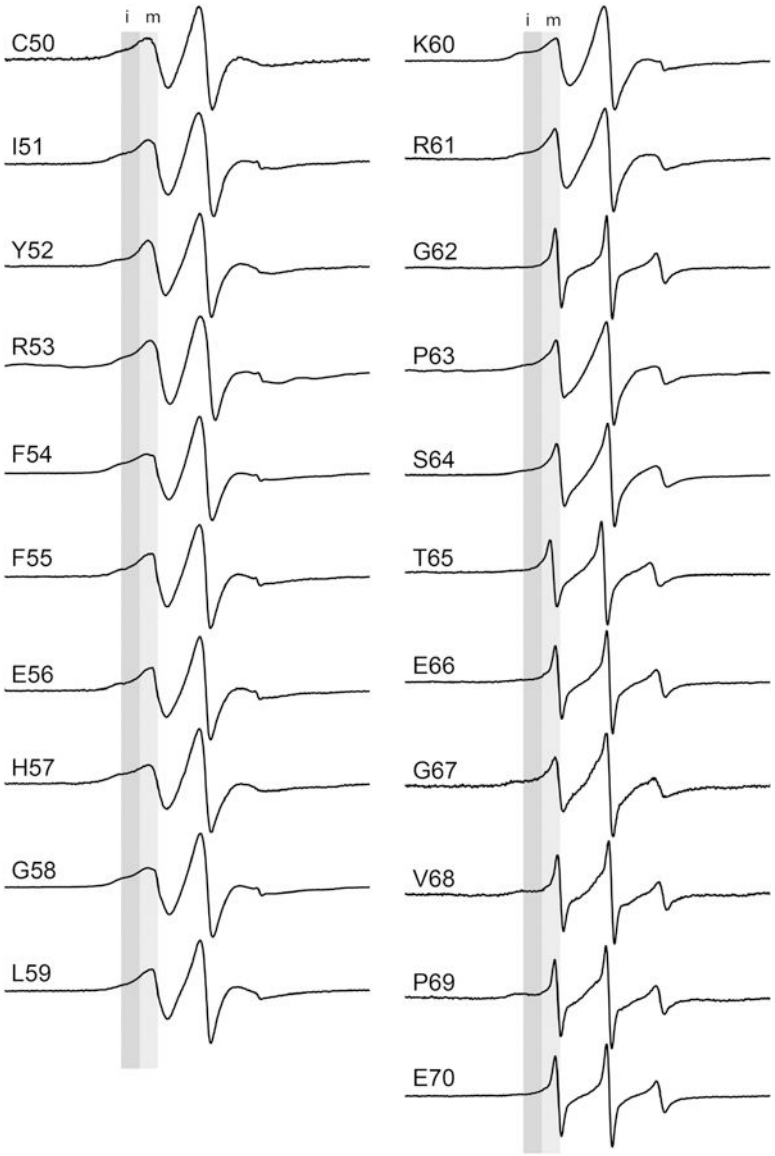

Figure 1.

CW X-band EPR spectra of full-length M2 protein for the indicated sites. Sites 50–60 were reported previously [22] and are part of the surface associated amphipathic helix. Light gray shading highlights mobile (m) peak components. Dark gray shading highlights immobile (i) peak components.

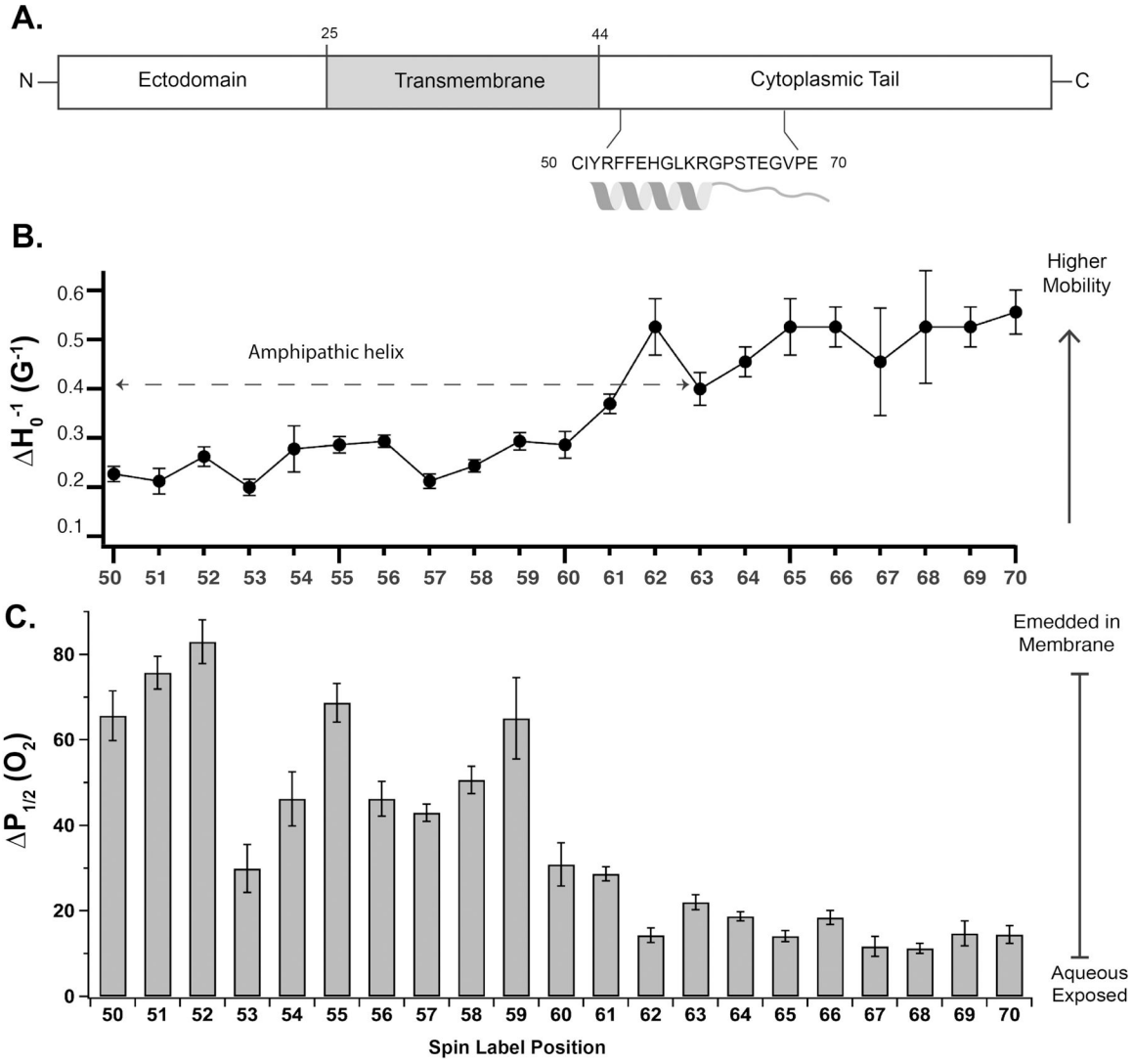

Fig. 2.

A. The domain structure of the full-length M2 protein. **B.** The relative mobility (inverse central line width, ΔH_0^{-1}) as a function of spin label position. The mobility factors were calculated from CWEPR spectra shown in Figure 1S. Sites 50–60 were previously published [22] and are included for comparison. Error bars represent the uncertainty in the position of the peak maxima and minima. **C.** Accessibility to oxygen measured by power saturation EPR as a function of spin label position. Error bars represent the 95% confidence intervals from the fits to the power saturation curves.

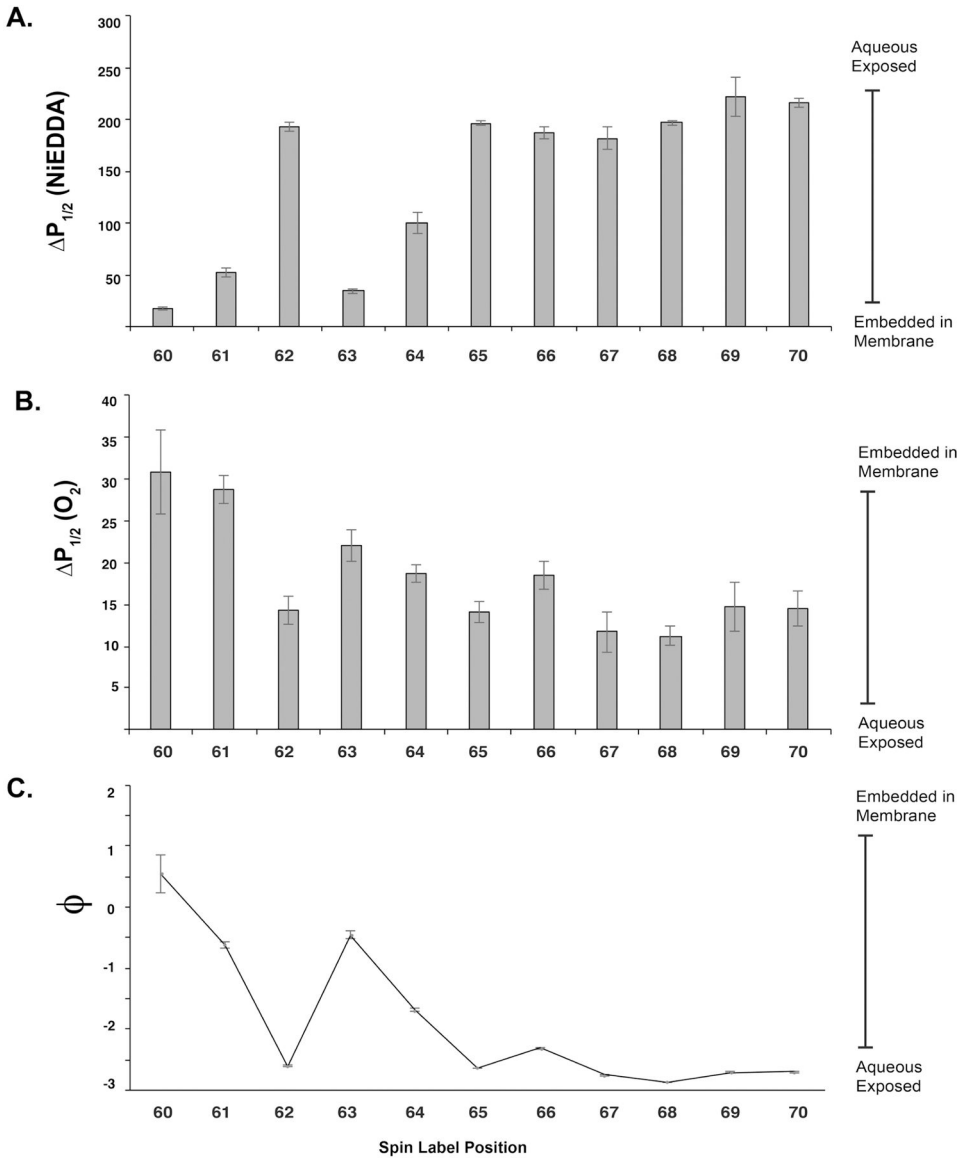

Fig. 3.

A. Accessibility to NiEDDA and **B.** O_2 as a function of spin label position for sites 60–70. Representative raw data for O_2 and NiEDDA accessibility measurements shown in Figure S1. Error bars represent the 95% confidence intervals from the fits to the power saturation curves. **C.** Contrast parameter, ϕ, calculated as described in the Materials and Methods.